Blunted neural and psychological stress processing predicts future grey matter atrophy in multiple sclerosis

Lil Meyer-Arndt[1], Stefan Hetzer[2], Susanna Asseyer[1], Judith Bellmann-Strobl[1,3], Michael Scheel[1], Jan-Patrick Stellmann[4,5,6], Christoph Heesen[4], Andreas K. Engel[7], Alexander U. Brandt[1], John-Dylan Haynes[1,2,8], Friedemann Paul[1,3,9,†], Stefan M. Gold [4,10,11,†] and Martin Weygandt[1,2,†,*]

Supplementary Material

[1] Charité – Universitätsmedizin Berlin, corporate member of Freie Universität Berlin, Humboldt-Universität zu Berlin, and Berlin Institute of Health, NeuroCure Clinical Research Center, 10117 Berlin, Germany.
[2] Charité – Universitätsmedizin Berlin, corporate member of Freie Universität Berlin, Humboldt-Universität zu Berlin, and Berlin Institute of Health, Berlin Center for Advanced Neuroimaging, 10117 Berlin, Germany.
[3] Max Delbrück Center for Molecular Medicine and Charité – Universitätsmedizin Berlin, corporate member of Freie Universität Berlin, Humboldt-Universität zu Berlin, and Berlin Institute of Health, Experimental and Clinical Research Center, 13125 Berlin, Germany.
[4] Institute of Neuroimmunology and Multiple Sclerosis (INIMS), Center for Molecular Neurobiology Hamburg, University Medical Center Hamburg-Eppendorf, 20251 Hamburg, Germany.
[5] Aix-Marseille Univ, CNRS, CRMBM, UMR 7339, Marseille Cedex, France
[6] APHM, Hopital de la Timone, CEMEREM, Marseille, France
[7] Department of Neurophysiology and Pathophysiology, University Medical Center Hamburg-Eppendorf, 20246 Hamburg, Germany.
[8] Charité – Universitätsmedizin Berlin, corporate Member of Freie Universität Berlin, Humboldt-Universität zu Berlin, Berlin Institute of Health, Bernstein Center for Computational Neuroscience, 10117, Berlin, Germany.
[9] Charité – Universitätsmedizin Berlin, corporate member of Freie Universität Berlin, Humboldt-Universität zu Berlin, and Berlin Institute of Health, Department of Neurology, 10117 Berlin, Germany.
[10] Charité – Universitätsmedizin Berlin, corporate member of Freie Universität Berlin, Humboldt-Universität zu Berlin, and Berlin Institute of Health, Department of Psychiatry and Psychotherapy, Campus Benjamin Franklin, 12203 Berlin, Germany.
[11] Charité – Universitätsmedizin Berlin, corporate member of Freie Universität Berlin, Humboldt-Universität zu Berlin, and Berlin Institute of Health, Department of Psychosomatic Medicine, 10117 Berlin, Germany.

† These authors contributed equally to this work.
* Corresponding author.
Charité – Universitätsmedizin Berlin, Charitéplatz 1, 10117 Berlin. Germany.
Email: martin.weygandt@charite.de

Materials and methods

Measurement of psychophysiological stress response markers

Heart rate

We used a standard pulse oximeter included in the Physiological Monitoring Unit of the MRI scanner to acquire pulse rates during experimental stages B and D. Compatible with our processing of fMRI data, only the last 8 min of stage D were evaluated for heart rate computation during stress. Details of heart rate determination including filtering are delineated in Weygandt *et al.* (2016). Based on a visual inspection of the filtered raw data, the quality of heart signals was considered sufficient for 20 of all 25 patients. The signals of these 20 patients were used for heart rate-related analyses, the data of the remaining five patients were considered as outliers and thus discarded.

Salivary cortisol

HPA-axis activity was assessed by salivary cortisol levels measured across the stress task (which took place in a constant time window between 3 and 7 pm across all pwMS to control for circadian variations). A salivary cortisol collection system (Sarsted, Germany) was used to acquire the samples. Specifically, participants were asked to keep the saliva collection device for 2 minutes in their mouth. Samples were stored at -80 °C until assayed using an Enzyme Linked Immunosorbent Assay (IBL, Germany). Salivary cortisol concentrations were measured in nanomoles per liter. Salivary cortisol data, which were already acquired in our recent cross-sectional study (10), were available for 13 out of 36 pwMS included in (10). For the subsample of 25 pwMS evaluated in the present longitudinal study, salivary cortisol data were available for 8 pwMS. Given that we were only interested in associations of immediate stress response markers and future atrophy in pwMS in this study (and not in an analysis of immediate and delayed

psychophysiological and neural stress responses as in [10]), we only evaluated cortisol data acquired during three stages in this longitudinal work (i.e., during A Pre-Baseline, C Pre-Stress, and E Post-Stress). Consistent with the other (neural and psychophysiological) stress response markers evaluated in the present work, salivary cortisol data acquired during an additional, delayed post-stress measurement in (10) were not analyzed.

MRI sequences

We acquired MR images of multiple sclerosis patients acquired during T0 and T1 with the same 3 Tesla whole-body tomograph (Magnetom Trio, Siemens, Erlangen, Germany) using a standard 12-channel head coil. For fMRI scans, we used a pseudo-continuous Arterial-Spin Labeling (ASL) Echo-Planar Imaging (EPI) sequence (Wang *et al.,* 2005) roughly covering the whole brain (22 ascending transversal slices, slice thickness 5.75 mm [including 15% inter-slice gap]; in-plane voxel resolution $3 \cdot 3$ mm^2; TR = 4000 ms; TE = 19ms; FA = 90°; FOV = $192 \cdot 192$ mm^2; matrix size = $64 \cdot 64$; label duration 1.5 sec, post-label delay 1.2 sec; phase-encoding direction anterior to posterior). One hundred and twenty images (60 control and 60 label) were acquired during the Rest stage (B; 8 minutes duration), 180 images (90 control, 90 label) during the Stress stage (D; 12 minutes duration).

In addition, two spin-echo EPI reference volumes with opposite phase encoding directions (anterior to posterior, posterior to anterior) were acquired in advance to the Rest and Stress ASL measurements with the same parameters as reported above to facilitate distortion correction of ASL images.

An anatomical T1-weighted sequence and a T2-weighted sequence were acquired with the following parameters: (T1) 176 slices; slice thickness 1.3 mm; in-plane voxel resolution $1.5 \cdot 1.5$ mm^2; TR = 1720 ms; TE = 2.34 ms; FA = 9°; FOV = $192 \cdot 192$ mm^2;

matrix size = 128 × 128; 1 minute and 43 seconds duration; (T2) 176 slices; 1 mm isotropic voxels; TR = 5000 ms; TE = 502 ms; FA = 120°; FOV = 256 · 256 mm^2; matrix size = 256 · 256; 5 minutes and 52 seconds duration.

Anatomical T1-weighted MRI scans of healthy controls were acquired at the University Medical Center Hamburg-Eppendorf in Hamburg using a 3 Tesla whole-body tomograph (Magnetom Skyra, Siemens, Erlangen, Germany) and a standard 32-channel head coil (256 slices; slice thickness 0.94 mm; in-plane voxel resolution 0.83 · 0.83 mm^2; TR = 2500 ms; TE = 2.12 ms; FA = 9°; FOV = 193 · 239 mm^2; matrix size = 232 × 288; 4 minutes and 57 seconds duration).

MRI preprocessing

Anatomical images

Lesion mapping

Supervised by a neuroradiologists, experienced raters manually generated patient-specific masks for voxels containing focal lesions with ITK-SNAP (http://www.itksnap.org) using patients' T2-weighted images.

Segmentation of T1-weighted anatomical brain images

To segment the brain of each participant and time point into areas of GM, white matter (WM), and cerebro-spinal fluid (CSF) we determined voxel images assessing the probability of each coordinate to belong to the three tissues with the combined spatial normalization and segmentation SPM12 (Wellcome Trust Centre for Neuroimaging, Institute of Neurology, UCL, London UK - http://www.fil.ion.ucl.ac.uk/spm) algorithm based on T1-weighted images. Coordinates containing lesioned tissue as reflected by the

lesion maps coregistered to the T1-weighted images were excluded. GM, WM, and CSF probability maps were computed once in the participant-specific ('native') image space and once in the anatomical Montreal Neurological Institute (MNI) standard space (Tzourio-Mazoyer *et al.,* 2002). The latter maps were adjusted for spatial deformations applied during the normalization which yielded 'modulated' tissue probability maps.

Determination of a GM group mask for fMRI analyses

To constrain our fMRI analyses to functional brain activity signals from healthy GM, we determined a group mask for this tissue in MNI-space which was derived from the modulated tissue probability maps of multiple sclerosis patients. Based on these maps, we computed the voxel-wise average modulated tissue probability for GM, WM and CSF across all patients. We then assigned each voxel to the tissue class for which the mean was maximal.

Coordinates which contained lesions according to the co-registered patient-specific lesion maps in at least one patient were excluded from the mask. Moreover, we removed the six direct neighbor voxels of each lesion voxels, i.e. voxel having a Euclidean distance of no more than one voxel to a given lesion coordinate to account for potential partial voluming effects. Finally, voxel coordinates located in the GM group mask that were covered by all fMRI scans of all patients were entered into the predictive functional MRI group analysis.

Determination of regional GM volume

For the computation of regional longitudinal GM atrophy, we determined the volume of the 122 GM areas included in the Neuromorphometrics atlas (defined in MNI-space and derived from the OASIS project; http://Neuromorphometrics.com; derived;

http://www.oasis-brains.org; distributed by SPM12) separately for T0 and T1 in four fully automated steps. Please note that the outcome of this automated procedure was validated by a neuroradiologist (M. S.).

First, we used the transformation parameters for co-registration of anatomical T1-weighted images from native to MNI-space (determined during segmentation) to perform an inverse co-registration. In particular, we registered the neuroanatomical atlas and the SPM12 templates for GM, WM, and CSF defined in MNI-space to the native T1-weighted image space.

In the second step, we assigned each voxel coordinate in native image space to one of the three tissue classes using their native space tissue probability maps as well as the tissue templates and lesion masks co-registered to the native T1-weighted image space. Specifically, a voxel was either assigned to GM (i.e. the target tissue type) i. if the probability for this tissue was larger than for WM and CSF based on the probabilistic tissue maps or ii. if the coordinate was simultaneously located in the manually determined and co-registered lesion mask and a GM area as determined by the co-registered GM group template. Please note that the latter step was necessary to determine the tissue class of voxels within lesions as the segmentation procedure does not yield reliable results for lesion coordinates. Please also note that we computed the GM volume measures in native T1-weighted image space to harness its high spatial resolution and thus reduce partial voluming effects.

In the third, we assigned each voxel coordinate classified as GM in the second step that was covered by the co-registered neuroanatomical atlas to its corresponding region in the atlas.

In the fourth step, we used a region growth algorithm to assign GM coordinates located inside the GM group mask but outside the co-registered atlas to one of the 122 GM

atlas regions. This was necessary as the co-registered atlas covered only approximately 80% of GM voxels due to individual anatomical variations. After the number of voxels was determined for each atlas region, we computed the regional GM volume by multiplying the number of voxels by the volume of a voxel in mm^3. Longitudinal volume differences (T1 minus T0) were then entered as criteria into our predictive fMRI analysis.

Functional images

In this study, we evaluated fMRI images that were already analyzed in Weygandt *et al.* (2016). Preprocessing of these images comprised six steps. Specifically, we first linearly co-registered the perfusion scans to spin-echo EPI reference volumes with anterior to posterior phase encoding direction measured in advance of each of the two fMRI blocks using the realignment algorithm of the SPM ASL processing software ASLtbx (Wang *et al.,* 2008). In the second step, we employed the FSL top-up algorithm (Andersson *et al.,* 2003) to remove spatial image distortions from the realigned ASL scans induced by B0-field inhomogeneities. Both spin-echo EPI reference images with opposing phase encoding direction were used in this procedure. In the third step, we linearly co-registered the preprocessed ASL images to the high-resolution anatomical T1-weighted scan of a patient. In the fourth step, images resulting from the previous were spatially smoothed with a three-dimensional isotropic Gaussian kernel at full width and half maximum of 8 mm. In the fifth step, we determined voxel images of the average regional cerebral blood flow (CBF; ml/100g/min) for the (final) 8 minutes of the rest and the stress measurement based on control-label pairs with ASLtbx (Wang *et al.,* 2008). Please note that only the final 8 minutes of the stress stage were used for averaging to control for scan duration across both conditions and task settings within the stress condition. Finally, we used the mapping parameters computed during segmentation of T1-weighted scans to register the

average regional CBF maps of both fMRI conditions to the MNI space. These spatially normalized regional CBF maps (voxel size of $3 \cdot 3 \cdot 3$ mm^3) computed for each patient and both fMRI conditions separately entered the fMRI group analysis (unlike contrast maps reflecting the regional CBF differences between stress and resting stage as in Weygandt *et al.,* 2016).

Statistical analyses

Longitudinal GM atrophy

Main effect of group on longitudinal GM atrophy

In the supplementary results section, we report results obtained in the second/factorial analysis presented in the analysis of longitudinal GM volume loss in the main text for the main effect of group on regional GM volume in all 122 areas. We report these findings in order to highlight GM regions affected by multiple sclerosis atrophy independent of the temporal dynamics of this process.

Psychophysiological stress task responses

Here, we test the suitability of the mental arithmetic stress paradigm to induce stress in terms of perceived psychological stress, heart rate, and salivary cortisol. Specifically, we used LME regression to evaluate whether perceived stress is higher during the post-stress (E) than the pre-stress rating stage (C) and whether our heart rate measure determined for the stress stage (D) is higher than that determined for rest (B). Again, patients' sex, age, progressive disease type, task load, and a fixed and random intercept were included in the model as covariates of no interest and permutation testing (10000 permutations of the task-stage vector / covariate of interest) was used for inference.

Stress-related variations in salivary cortisol release across experimental stages in pwMS were evaluated in a very similar fashion. Contrary to the analysis of perceived stress and heart rate, however, we decided to model cortisol data across the three respective stages (i.e., A Pre-Baseline, C Pre-Stress, and E Post-Stress) in each of the two LME regression analysis conducted to account for the smaller number of samples available (i.e., N = 8) and thus to increase the power of the analyses. Specifically, we used a dichotomous covariate of interest coding 1 for stage E and 0 for stages A and C to contrast differences in cortisol release between the post-stress vs. both pre-stress stages in a first LME analysis. Motivated by findings showing that an MRI scanning session can act as a potent stressor/trigger for cortisol release independent of the stimuli applied and that this stressor can trigger a maximal cortisol release at session (i.e., stressor) onset which is then followed by a continuous decline in release across the session (Muehlhan et al., 2011), we then proceeded by testing an alternative covariate of interest in a second analysis. Specifically, the respective regressor of interest in this analysis coded 1 for stage A, 2 for C, and 3 for E to evaluate whether such a continuous decline in cortisol release is also present in our data. As for perceived stress and heart rate, patients' sex, age, progressive disease type, task load, and a fixed and random intercept were included in the model as covariates of no interest in both cortisol data analyses.

Predicting future multiple sclerosis GM atrophy based on neural stress responses

Computation of neural network stress responses

In this analysis, we tested whether task-induced activity changes of neural networks predict longitudinal GM volume differences (i.e., for T1 – T0) in regions subject to GM atrophy in pwMS. The predictors of interest for this analysis, the neural network stress response parameters, were computed in three steps.

In the first, we determined neural networks based on patients' brain activity during the stress stage with SVD, a signal processing technique widely applied for the analysis of complex multivariate biological data (Wall *et al.*, 2003; Mourao-Miranda *et al.,* 2005). Specifically, SVD decomposes a given set of manifest/directly measurable data represented by matrix **X** into three matrices **U**, **S** and **V**. In the present study, the elements of **X** reflect the average CBF for each participant (one participant per matrix row) and 121 regions (one region per matrix column) comprised in the Neuromorphometrics atlas. (Please note that in contrast to our anatomical data only 121 regions could be evaluated for fMRI as a single small inferior cerebellar area (i.e. Vermal Lobules VIII-X) was not covered across all patients by the ASL fMRI sequence.) More specifically, matrix $\mathbf{X}_{\text{Rest}}$ contained these data for the resting measurement while matrix $\mathbf{X}_{\text{Stress}}$ contained the data for stress. After the average regional CBF values for both matrices were determined, they were standardized (i.e., centered) patient-wise by subtracting the average CBF of a given patient across all 121 regions during a given task stage. After applying SVD to $\mathbf{X}_{\text{Stress}}$, we obtained $\mathbf{U}_{\text{Stress}}$, $\mathbf{S}_{\text{Stress}}$ and $\mathbf{V}_{\text{Stress}}$. The columns of $\mathbf{U}_{\text{Stress}}$ contain the principal components of $\mathbf{X}_{\text{Stress}}$ which reflect the characteristic variation of network activity (one column per network) across participants (one column element per patient). This characteristic variation underlies the signals of individual regions (columns in $\mathbf{X}_{\text{Stress}}$) depending on the relatedness between a given region and network. The relatedness between a given network and all included regions of interest is reflected in a network-specific column of $\mathbf{V}_{\text{Stress}}$ which is frequently called the matrix of Eigenimages of raw data (e.g., Mourao-Miranda *et al.,* 2005). Finally, $\mathbf{S}_{\text{Stress}}$ corresponds to the matrix of singular values which reflect the strength of the contribution of each of the PC activity signals to the activity of all regions. Importantly, it is possible to reconstruct the raw data (here: the centered CBF

signals of individual regions) from the 'latent' variables determined by SVD by computing $\mathbf{X} = \mathbf{U} \cdot \mathbf{S} \cdot \mathbf{V}^T$.

As we were interested in differential network activity (i.e. network activity differences for stress minus rest), we computed the activity of our networks during the resting stage in the second step. Specifically, we used the Eigenimages and the matrix of singular values determined for stress and the centered regional CBF signals for rest and computed $\mathbf{U}^*_{Rest} = \mathbf{X}_{Rest} \cdot (\mathbf{S}_{Stress} \cdot \mathbf{V}^T_{Stress})^+$. In this equation, $(\mathbf{S}_{Stress} \cdot \mathbf{V}^T_{Stress})^+$ corresponds to the Moore-Penrose pseudoinverse of $\mathbf{S}_{Stress} \cdot \mathbf{V}^T_{Stress}$.

In the third step, we determined the differential network activity for stress minus rest by computing $\mathbf{\Delta U} = \mathbf{U}_{Stress} - \mathbf{U}^*_{Rest}$. Please note that it was impossible to determine differential activity by simply calculating $\mathbf{\Delta U} = \mathbf{U}_{Stress} - \mathbf{U}_{Rest}$ (i.e. using network activity $\mathbf{U}_{Rest}$ as determined by SVD of $\mathbf{X}_{Rest}$) as the principal components identified by SVD are based on the correlations (i.e. 'connectivity') between regions. Since these correlations differ for $\mathbf{X}_{Rest}$ and $\mathbf{X}_{Stress}$ (compare Fig. 3a), the PCs (i.e. neural networks) identified by SVD of $\mathbf{X}_{Rest}$ would not have been the same as the PCs identified by SVD of $\mathbf{X}_{Stress}$. See Fig. S1 below for an illustration of the procedure.

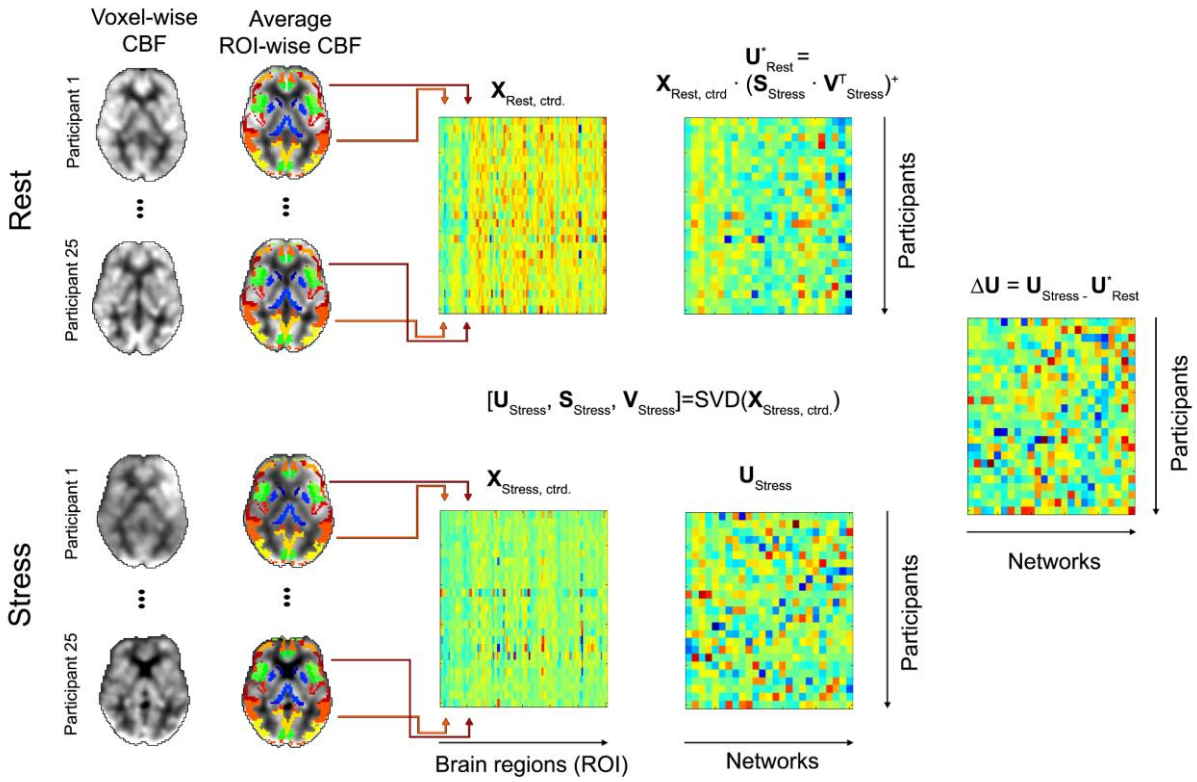

Figure S1 illustrates the network parameter computation method. Abbrev.: ctrd., centered; For details, see text.

<u>Determination of brain regions contributing significantly to the activity of networks</u>

To identify areas contributing significantly to the activity of networks described above, we used permutation testing (10000 permutations). In each permutation, all rows of each column of $\mathbf{X}_{Stress}$ were permuted independently first. Then, we computed the SVD of the permuted version of $\mathbf{X}_{Stress}$ and pooled all resulting elements of $\mathbf{V}_{Stress}$ across all permutations. Finally, we only considered those regions as significantly contributing to a given network which had a $\mathbf{V}_{Stress}$-score (computed based on non-permuted $\mathbf{X}_{Stress}$) smaller than the value with the 2.5% smallest value in the $\mathbf{V}_{Stress}$-score distribution or larger than the value with the 2.5% largest value in this distribution (cf. Mourao-Miranda *et al.,* 2005).

Stress network activity differences between persons with MS and controls To test whether atrophy-predictive neural network activity (i.e., of the 18th and the 22nd network; see Results) was characterized by hyper- or hypoactivity in MS, we compared the differential stress network activity parameters for pwMS (i.e., columns in **ΔU** for the 18th and the 22nd neural network; see 'Computation of neural network stress responses' above) with the corresponding factors computed for the persons included in the fMRI control group. Specifically, we first computed $\mathbf{U}^*_{\text{Rest HC}} = \mathbf{X}_{\text{Rest HC}} \cdot (\mathbf{S}_{\text{Stress MS}} \cdot \mathbf{V}^T_{\text{Stress MS}})^+$ and $\mathbf{U}^*_{\text{Stress HC}} = \mathbf{X}_{\text{Stress HC}} \cdot (\mathbf{S}_{\text{Stress MS}} \cdot \mathbf{V}^T_{\text{Stress MS}})^+$ based on the fMRI data of the fMRI control group. In the next step, we subtracted $\mathbf{U}^*_{\text{Rest HC}}$ from $\mathbf{U}^*_{\text{Stress HC}}$ to obtain differential stress network responses **ΔU** in HCs.

After these differential activity parameters were determined, we conducted robust regression analyses testing differences of these parameters between pwMS and persons in the fMRI control group for both networks. Specifically, a dichotomous regressor coding ones for pwMS and zeros for HCs served as covariate of interest. Participants' sex, age, and whether or not a progressive MS was present (plus constant) served as covariates of no interest. Again, permutation testing was used for inference (10000 permutations of the covariate of no interest).

Predicting future GM atrophy in MS based on stress-related cortisol release

In this analysis, we tested with robust regression whether the difference in cortisol release post-stress minus pre-stress (covariate of interest) in eight pwMS predicts the future atrophy of right superior parietal lobule and of right exterior cerebellum. Again, patients' regional GM volume at T0, sex, age, the presence of progressive MS, task load,

and a constant served as covariates of no interest. Permutation testing was used for inference (10000 permutations).

Associations between stress-related cortisol release, atrophy-predictive neural network activity, and perceived stress in MS

Here, we evaluated in two analyses using robust regression whether stress-related cortisol release across patients is related to differential brain activity of each of the two atrophy-predictive networks (18 and 22). Specifically, differential activity of each network was treated as covariate of interest once. Variations in cortisol release post-stress minus pre-stress across patients served as criterion, and patients' sex, age, the presence of progressive MS, task load (plus constant) as covariates of no interest. Permutation testing (10000 permutations) was used for inference.

Finally, we also tested whether the mentioned differences in cortisol release for stress minus rest are related to perceived stress. Except for the fact that perceived stress served as covariate of interest, all aspects were identical to the two analyses conducted for modelling based on neural network activity.

Results

Demographic and clinical participant characteristics

An LME analysis showed that the EDSS (corrected for sex, age, progressive disease type [y/n], fixed and random intercept) did not vary significantly across time according to a two-sided threshold of $\alpha = 0.05$ ($t_{45} = -0.45$, $p = 0.669$). The volume of T2-weighted lesions was Md = 4.61 cm^3 (Rg: 0.09 – 48.91 cm^3) at T0 and Md = 5.68 cm^3 (Rg: 0.17 – 49.34 cm^3) at T1. According to a longitudinal LME analysis and to a two-sided threshold of $\alpha = 0.05$ this increase (evaluated based on log-transformed lesion volume computed via ln [lesion volume + 0.001] and corrected for the same covariates of no interest as used for EDSS) was significant ($t = 3.50$, $p = 0.002$).

To evaluate the inflammatory disease activity preceding study participation, a neuroradiologist (M. S.) compared a T2w MRI brain scan acquired within a median time period of 321 days (Rg = 169 – 435 days) before the baseline visit T0 (available for 15 PwMS) to the corresponding T2w scan acquired at T0. The comparison showed that only three PwMS had developed new lesions in this pre-study period (Md = 0 new lesions; Rg = 0 - 4 new lesions). Moreover, the median number of days since the end of the last relapse before T0 across all 25 PwMS was 657 days (Rg = 50 – 3550 days). Thus, the inflammatory disease activity prior to study participation at T0 was small.

Longitudinal GM volume loss

Fig. S2 below shows the regions in the atlas with significantly different GM volume in patients than controls across both time points or areas with a significant main effect of group on regional GM volume in the factorial analysis presented in the main text respectively.

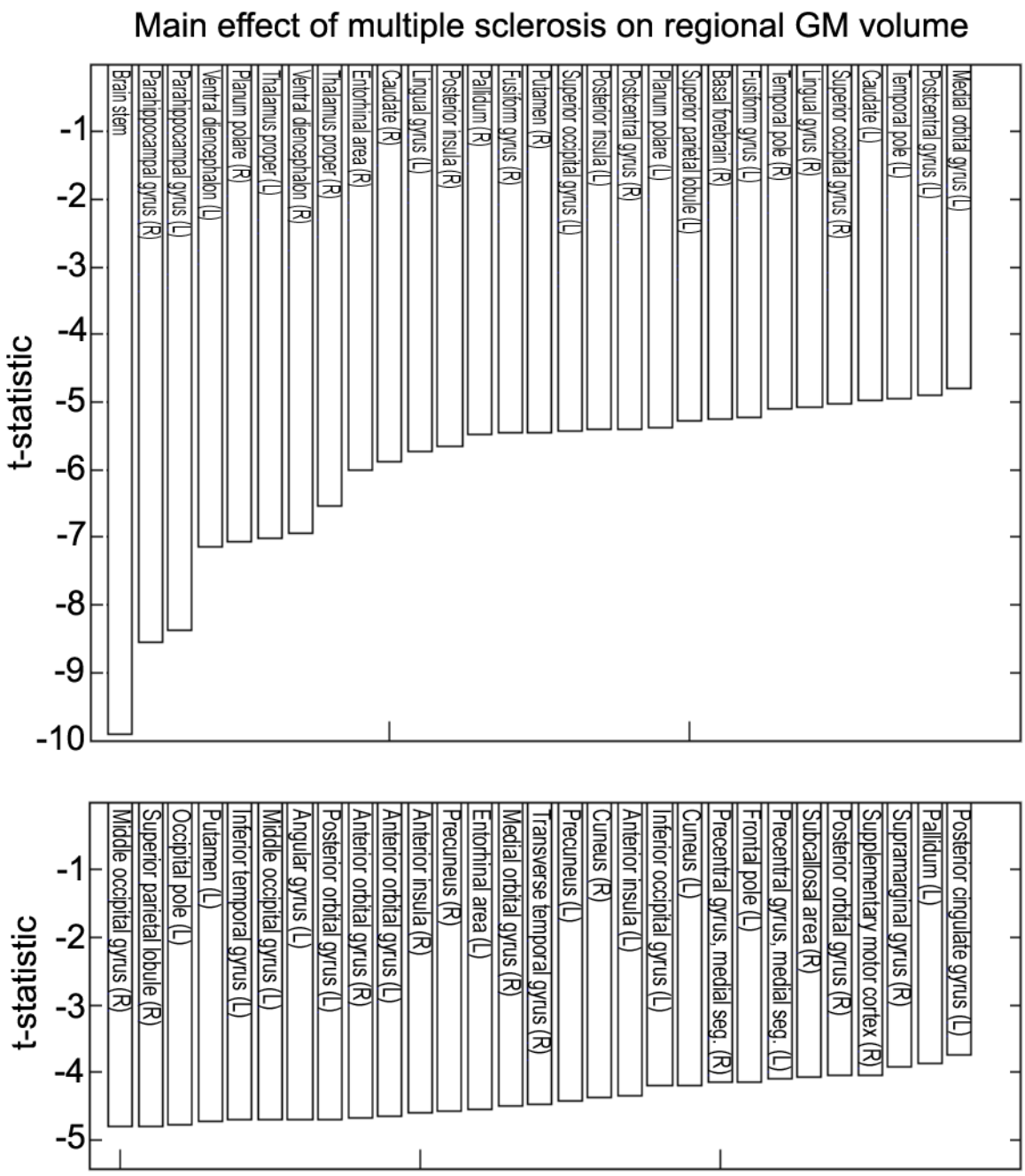

Figure S2 depicts the main effect of group on GM volume across both time points. All areas identified with the two-sided test and $a_{FWE} = 0.05 / 122 = 4.1 \cdot 10^{-4}$ indicated areas with less GM volume in patients than controls.

Psychophysiological stress task responses

These supplementary analyses confirmed that the task also induced stress on the level of the two psychophysiological stress response measures heart rate and perceived stress. In particular, the median level of perceived stress increased from 2 during pre-stress to 5 during post-stress ($t = 2.5$, $p = 0.012$). Moreover, the median heart rate increased form 73 beats per minute during the rest to 77 during the stress stage ($t = 5.0$, $p < 10^{-4}$). Results for the supplementary analyses evaluating the relation of stress and salivary cortisol release are shown in the below Figure S3.

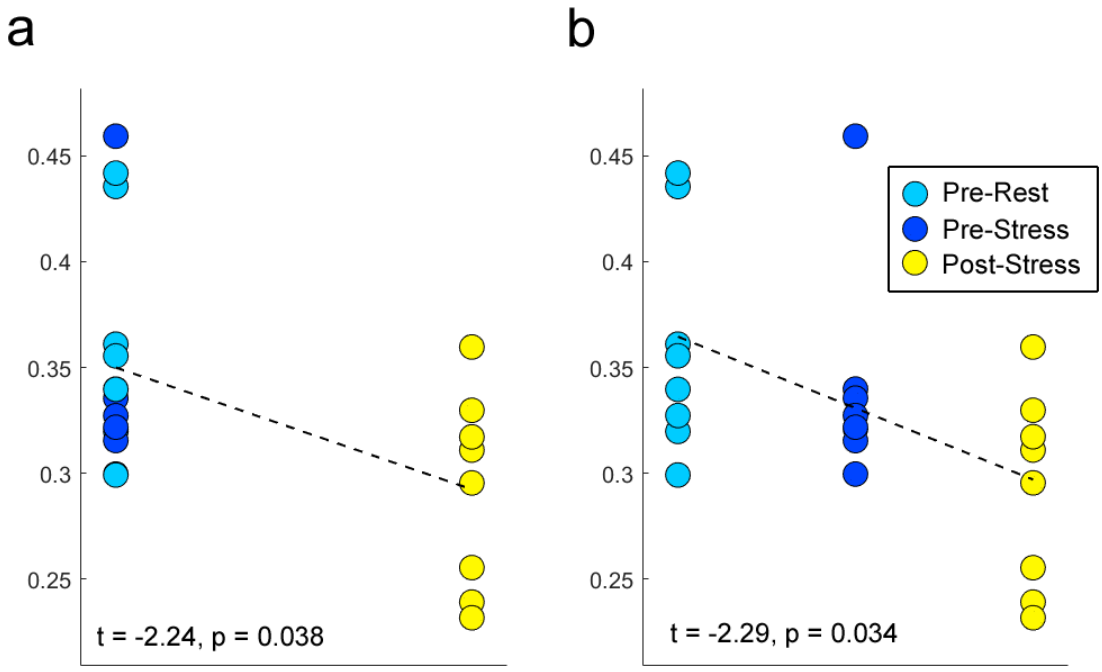

Figure S3. Relation of stress and salivary cortisol release. (a) depicts the association between the dichotomous regressor coding 1 for the post-stress (E) and 0 for both pre-stress conditions (A, C). Moreover, (b) shows the association between a linear regressor coding 1 for stage A, 2 for C, and 3 for E. In both panels (a) and (b), the criterion was corrected for covariates of no interest.

Stress network activity differences between patients and controls

This analysis showed that neither the stress-evoked activity of the 18th nor the activity of the 22nd network (which were both predictive of future atrophy in pwMS) differed from

the activity of the corresponding networks in the 21 persons included in the fMRI control group. Specifically, for the 18th network we computed t = -0.46, p = 0.641. Moreover, for the 22nd network we obtained t = 0.74 and p = 0.455. Figure S4 shows the t-statistics obtained for the group difference across all 25 networks.

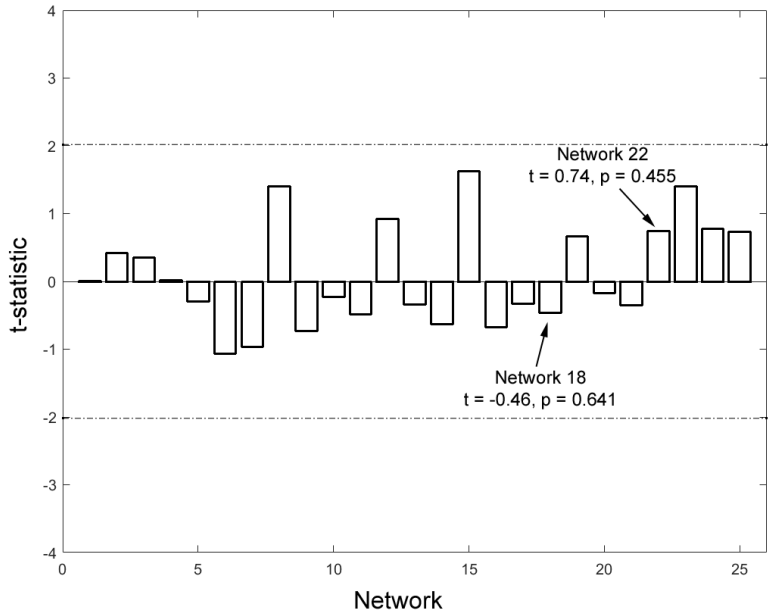

Figure S4 depicts differences between pwMS and persons in the fMRI control group in terms of differential, stress-evoked network activity at T0. The dash-dotted line highlights an undirected threshold (α = 0.05) derived from the t-distribution for 41 degrees of freedom.

Predicting future GM atrophy in MS based on stress-related cortisol release

This analysis suggests that neither the longitudinal volume loss in right superior parietal lobule nor that of right exterior cerebellum could be predicted based on stress-related salivary cortisol secretion during the mental arithmetic task conducted at T0. Figure S5 below illustrates these results.

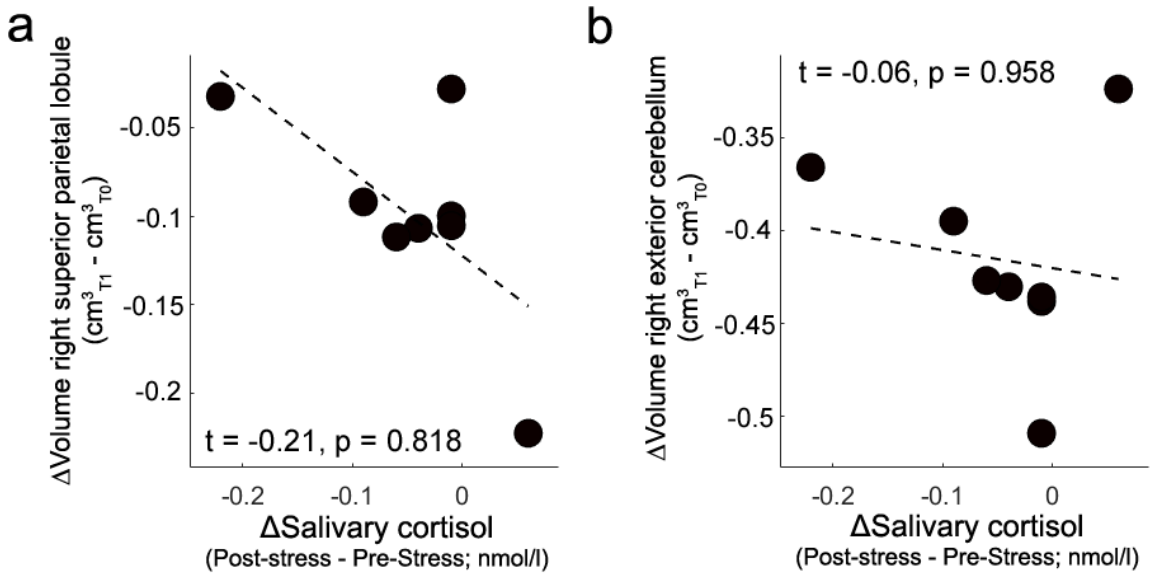

Figure S5. The panel on the left (a) depicts modelling volume differences T1 – T0 in the right superior parietal lobule based on differences in salivary cortisol secretion for Post-stress – Pre-stress, whereas (b) depicts this for the right exterior cerebellum. In both panels (a) and (b), the criterion was corrected for covariates of no interest.

Associations between stress-related cortisol release, atrophy-predictive neural network activity, and perceived stress in MS

Relating stress-related cortisol releases to differential activity of atrophy-predictive networks showed that activity of the 18th network was negatively associated with differential salivary cortisol release according to an undirected test (t = -4.18, p = 0.045). See Figure S6.

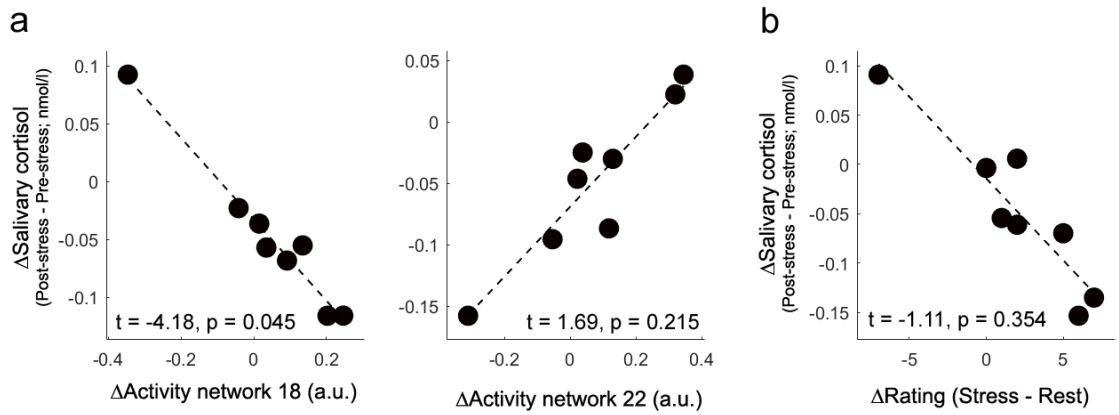

Figure S6. (a) depicts the results for modelling differential salivary cortisol release based on differential activity of the 18th network (left graph) or differential activity of the 22nd network respectively (right graph). In (b), differential salivary cortisol release was modelled based on differential perceived stress ratings. In all depicted panels, the criterion was corrected for covariates of no interest.

References

Andersson JL, Skare S, Ashburner J. How to correct susceptibility distortions in spin-echo echo-planar images: application to diffusion tensor imaging. Neuroimage 2003, 20, 870-88.

Mourao-Miranda J, Bokde AL, Born C, Hampel H, Stetter M. Classifying brain states and determining the discriminating activation patterns: Support Vector Machine on functional MRI data. NeuroImage 2005, 28, 980-95.

Muehlhan M, Lueken U, Wittchen H-U, Kirschbaum C. The scanner as a stressor: Evidence from subjective and neuroendocrine stress parameters in the time course of a functional magnetic resonance imaging session. Int. J. Psychophysiol. 2011; 79(2):118-26.

Tzourio-Mazoyer N, Landeau B, Papathanassiou D, Crivello F, Etard O, Delcroix N, et al. Automated anatomical labeling of activations in SPM using a macroscopic anatomical parcellation of the MNI MRI single-subject brain. Neuroimage 2002, 15, 273-89.

Wall ME, Rechtsteiner A, Rocha LM. Singular value decomposition and principal component analysis. In A Practical Approach to Microarray Data Analysis (D.P. Berrar, W. Dubitzky, M. Granzow, eds.) Kluwer: Norwell, MA, 2003. pp. 91-109. LANL LA-UR-02-4001.

Wang J, Rao H, Wetmore GS, Furlan PM, Korczykowski M, Dinges DF, Detre JA. Perfusion functional MRI reveals cerebral blood flow pattern under psychological stress. Proc Natl Acad Sci U S A 2005, 102, 17804-9.

Wang Z, Aguirre GK, Rao H, Wang J, Fernandez-Seara MA, Childress AR, et al. Empirical optimization of ASL data analysis using an ASL data processing toolbox: ASLtbx. Magn Reson Imaging 2008, 26, 261-9.

Weygandt M, Meyer-Arndt L, Behrens JR, Wakonig K, Bellmann-Strobl J, Ritter K, et al. Stress-induced brain activity, brain atrophy, and clinical disability in multiple sclerosis. Proc Natl Acad Sci U S A 2016, 113, 3444-9.